Report

SOURCE DATA | TRANSPARENT PROCESS

EMBO reports

miR-424/503 modulates Wnt/β-catenin signaling in the mammary epithelium by targeting LRP6

Erin A Nekritz[1,†], Ruth Rodriguez-Barrueco[2,3,*,†], Koon-Kiu Yan[4], Meredith L Davis[2,5], Rachel L Werner[1], Laura Devis-Jauregui[2], Partha Mukhopadhyay[1], Jiyang Yu[4], David Llobet-Navas[2,6,**] & Jose Silva[1,***]

Abstract

During the female lifetime, the expansion of the epithelium dictated by the ovarian cycles is supported by a transient increase in the mammary epithelial stem cell population (MaSCs). Notably, activation of Wnt/β-catenin signaling is an important trigger for MaSC expansion. Here, we report that the miR-424/503 cluster is a modulator of canonical Wnt signaling in the mammary epithelium. We show that mammary tumors of miR-424(322)/503-depleted mice exhibit activated Wnt/β-catenin signaling. Importantly, we show a strong association between miR-424/503 deletion and breast cancers with high levels of Wnt/β-catenin signaling. Moreover, miR-424/503 cluster is required for Wnt-mediated MaSC expansion induced by the ovarian cycles. Lastly, we show that miR-424/503 exerts its function by targeting two binding sites at the 3'UTR of the LRP6 co-receptor and reducing its expression. These results unveil an unknown link between the miR-424/503, regulation of Wnt signaling, MaSC fate, and tumorigenesis.

Keywords breast cancer; LRP6; miR-424/503; Wnt/β-catenin
Subject Categories Cancer; RNA Biology; Signal Transduction
DOI 10.15252/embr.202153201 | Received 5 May 2021 | Revised 3 September 2021 | Accepted 10 September 2021 | Published online 11 October 2021
EMBO Reports (2021) 22: e53201

Introduction

The mammary gland is a very dynamic organ that undergoes continuous tissue remodeling during the female lifetime (Macias & Hinck, 2012). Expansion and regression of the mammary epithelium dictated by the ovarian hormones involve alternating cycles of cell death and proliferation. During this process, enlargement of the epithelial compartment is supported by a transient increase in the mammary epithelial stem cell population (MaSC) (Asselin-Labat *et al*, 2010; Joshi *et al*, 2010). These cycles are tightly regulated in time and space to ensure proper organ function and avoid pathological consequences.

Numerous studies have elucidated some of the major signaling events within the mammary epithelium. For instance, TGF-β has been implicated as a negative regulator of proliferation during ductal elongation (Macias & Hinck, 2012). The induction of apoptosis via the Jak/Stat pathway and several matrix metalloproteinases (MMPs) is involved in the remodeling of the mammary epithelium during involution (Watson, 2006), and RANK ligand is critical for lobuloalveologenesis (Fernandez-Valdivia *et al*, 2009). Importantly, canonical Wnt signaling via β-catenin has been also shown to be essential for mammary gland development (Alexander *et al*, 2012). Specifically, paracrine Wnt signaling mediated by multiple Wnt ligands induces mammary epithelial expansion through its effect on MaSCs (Rajaram *et al*, 2015). In these cells, the expression of Wnt co-receptors LRP5 and LRP6 is the limiting factor for canonical Wnt signaling (Alexander *et al*, 2012; Goel *et al*, 2012). Remarkably, deregulation of Wnt/β-catenin signaling in the mammary gland induces pathological consequences, and hyperactivation of this pathway has been found in some aggressive breast cancer subtypes (Xu *et al*, 2020). Despite the above, our understanding of how canonical Wnt signaling is properly regulated to maintain mammary gland homeostasis is far from complete.

Recently, we investigated the landscape of miRNAs expressed in the mammary epithelium and found that the miR-424(322)/503 is a TGF-β-induced regulator of involution in the mammary epithelium (Llobet-Navas *et al*, 2014a). This cluster expresses two microRNAs, miR-424(miR-322 in mice) and miR-503, that belong to the miR-16 family (Rissland *et al*, 2011). We found that this microRNA cluster is commonly lost in 14% of breast cancers acting as a tumor

1 Graduate School, Department of Pathology, Icahn School of Medicine at Mount Sinai Hospital, New York, NY, USA
2 Molecular Mechanisms and Experimental Therapy in Oncology-Oncobell Program, Bellvitge Biomedical Research Institute (IDIBELL), L'Hospitalet de Llobregat, Barcelona, Spain
3 Anatomy Unit, Department of Pathology and Experimental Therapy, School of Medicine, University of Barcelona (UB), L'Hospitalet de Llobregat, Barcelona, Spain
4 Department of Computational Biology, St. Jude Children's Research Hospital, Memphis, TN, USA
5 Department of Pathology, Duke University School of Medicine, Durham, NC, USA
6 Centro de Investigación Biomédica en Red de Cáncer (CIBERONC), Instituto de Salud Carlos III (ISCIII), Madrid, Spain
*Corresponding author. Tel: +34 689 54 93 90; E-mail: rrodriguezb@idibell.cat
**Corresponding author. Tel: +34 695 80 74 92; E-mail: dllobet@idibell.cat
***Corresponding author. Tel: +1 212 659 5618; E-mail: jose.silva@mssm.edu
†These authors contributed equally to this work

suppressor (Rodriguez-Barrueco *et al*, 2017). The deletion of the miR-424/503 locus is associated with the triple-negative subtype and with poor prognosis characteristics. The miR-424/503 locus is in chromosome X and is monoallelically expressed due to X chromosome inactivation. In breast cancers, the active allele is the allele selectively deleted, whereas the methylated inactive one remains intact. Finally, we also reported that miR-424(322)/503 knockout mice develop mammary tumors over time that are promoted by pregnancy (Rodriguez-Barrueco *et al*, 2017). Remarkably, we noticed that tumors emerging in miR-424(322)/503$^{-/-}$ mice presented phenotypical characteristics found in tumors with activated canonical Wnt signaling. Thus, we decided to investigate a potential link between the loss of miR-424/503 and the Wnt/β-catenin pathway. Here, we report that the miR-424/503 cluster is a novel modulator of the canonical Wnt signaling in the mammary epithelium that exerts its function by decreasing the expression of the LRP6 co-receptor. Additionally, we also show that the loss of this miR cluster is associated with breast cancers with hyperactivation of Wnt/β-catenin signaling.

Results and Discussion

Deletion of miR-42(322)/503 is associated with breast cancers with hyperactivation of canonical Wnt signaling

Commonly, mammary tumors emerging in transgenic mice expressing potent oncogenes present aggressive anaplastic and metaplastic characteristics (Li *et al*, 2003). In the cases where some differentiated characteristics are present, these tumors tend to express defined markers of luminal or basal cancers but rarely both (Pfefferle *et al*, 2013). In contrast to this, we observed that tumors emerging in miR-424/503$^{-/-}$ mice were moderately differentiated and comprised of ducts with layers of epithelial cells showing a high nucleus-to-cytoplasm ratio and extensive fibrosis (Fig 1A). Additionally, immunohistochemistry staining with cytokeratin (CK) markers revealed that these tumors contained a mix of both luminal and basal cell types (Fig EV1A). As these characteristics resemble tumors with activated Wnt/β-catenin signaling (Li *et al*, 2003; Liu *et al*, 2004), we decided to investigate the staining of β-catenin and CK6, a marker associated with precursor cells that are found in tumors with hyperactivated canonical Wnt signaling (Li *et al*, 2003). Remarkably, we found strong immunohistochemistry staining (IHC) of both markers including accumulation of nuclear β-catenin in miR-424/503$^{-/-}$ tumors (Figs 1A and EV1B). Accumulation of nuclear β-catenin was not only detected in tumors emerging in miR-424(322)/503 knockout mice, and positive staining was also observed in young knockout animals (4–6 months old) before tumors emerged (Fig EV1C).

We have previously reported that the miR-424/503 locus is deleted in ~14% of all breast cancers and that this correlates with lower expression of both miR-424 and miR-503 (Rodriguez-Barrueco *et al*, 2017). Thus, we reasoned that we could investigate the link between the miR-424/503 and canonical Wnt signaling in human samples by evaluating the accumulation of β-catenin in breast cancers with deletion and/or reduced expression of the miR cluster. For this, we analyzed the reverse-phase protein array (RPPA) data that are available for the BRCA-TCGA data set (Cancer Genome Atlas, 2012) and that contain information regarding β-catenin expression at a protein level. In agreement with the observation in mice, both deletion and low expression of miR-424/503 were associated with accumulation of β-catenin (Figs 1B and C, and EV1D). Additionally, we performed gene set enrichment analysis to investigate whether this high level of β-catenin impacts the activity of Wnt signaling. As expected, a significant increase in Wnt targets was found in tumors deficient in miR-424/503 expression (Fig 1D). Importantly, this association was confirmed when an independent breast cancer data set containing CNA and expression data for over 2,500 samples (METABRIC (Curtis *et al*, 2012)) was analyzed (Fig 1D). It is well known that a fraction of human breast cancers enriched in triple-negative characteristics has hyperactivation of Wnt signaling (Pohl *et al*, 2017). However, alterations in signaling components that are commonly found mutated in other tumors (e.g., APC, β-catenin) are rare in breast tumors (Sanchez-Vega *et al*, 2018). Genomics analysis has recently classified triple-negative breast cancers (TNBCs) in at least four subtypes with different molecular characteristics (Lehmann *et al*, 2011, 2016). Remarkably, these include two subtypes (~ 50% of all TNBCs), basal-like 2 (BL2) and mesenchymal (M), characterized by signatures of epithelial–mesenchymal transition and hyperactivation of Wnt signaling (Lehmann *et al*, 2011, 2016). Thus, we wondered whether deletion of miR-424/503 could be associated with these molecular subtypes. Remarkably, we found a strong association of miR-424/503 deletion with the BL2 and M subtypes (Fig 1E).

Overall, all the above suggest that deregulation of miR-424/503 influences canonical Wnt signaling and that deletion of this microRNA cluster is associated with breast cancers with hyperactivation of Wnt signaling. Prompted by these results, we decided to further investigate the existence of a causal link between miR-424/503 and the canonical Wnt signaling.

miR-424(322)/503 regulates Wnt/β-catenin activity in MaSCs

In the mammary gland, Wnt/β-catenin signaling is a critical regulator of epithelial tree homeostasis (Alexander *et al*, 2012). During regular ovarian cycles and pregnancy, elevated hormonal level promotes secretion of Wnt ligands in the luminal cells, which in turn induces the expansion of MaSCs (Joshi *et al*, 2010; Diaz-Guerra *et al*, 2012). Expansion of MaSCs supports the enlargement of the mammary epithelial compartment. Previously, we have reported that miR-424(322)/503 is expressed at a low level in resting luminal and basal mammary epithelial subpopulations (Llobet-Navas *et al*, 2014a,b). Remarkably, deletion of this miR cluster generated enlarged terminal ductal lobular units (TDLUs) that are more evident during the diestrus phase and after pregnancy in young animals (4–8 months old). Older animals presented epithelial lesions compatible with alveolar hyperplasia. Finally, invasive carcinomas emerge in animals that are ~ 1 year old (Llobet-Navas *et al*, 2014a). Based on the new data connecting this cluster with Wnt signaling, we decided to look in more detail at its expression in MaSCs. For this, we purified the basal, luminal, and the enriched MaSC subpopulation from 4- to 6-month-old WT FVB female mice in the estrus and diestrus phase; then, expression of miR-424(322) and miR-503 was assessed by qRT–PCR. In brief, non-epithelial cells were removed from single-cell suspension by incubation with CD31-, CD-45-, Ter119-, and BP-1-biotin. The remaining epithelial

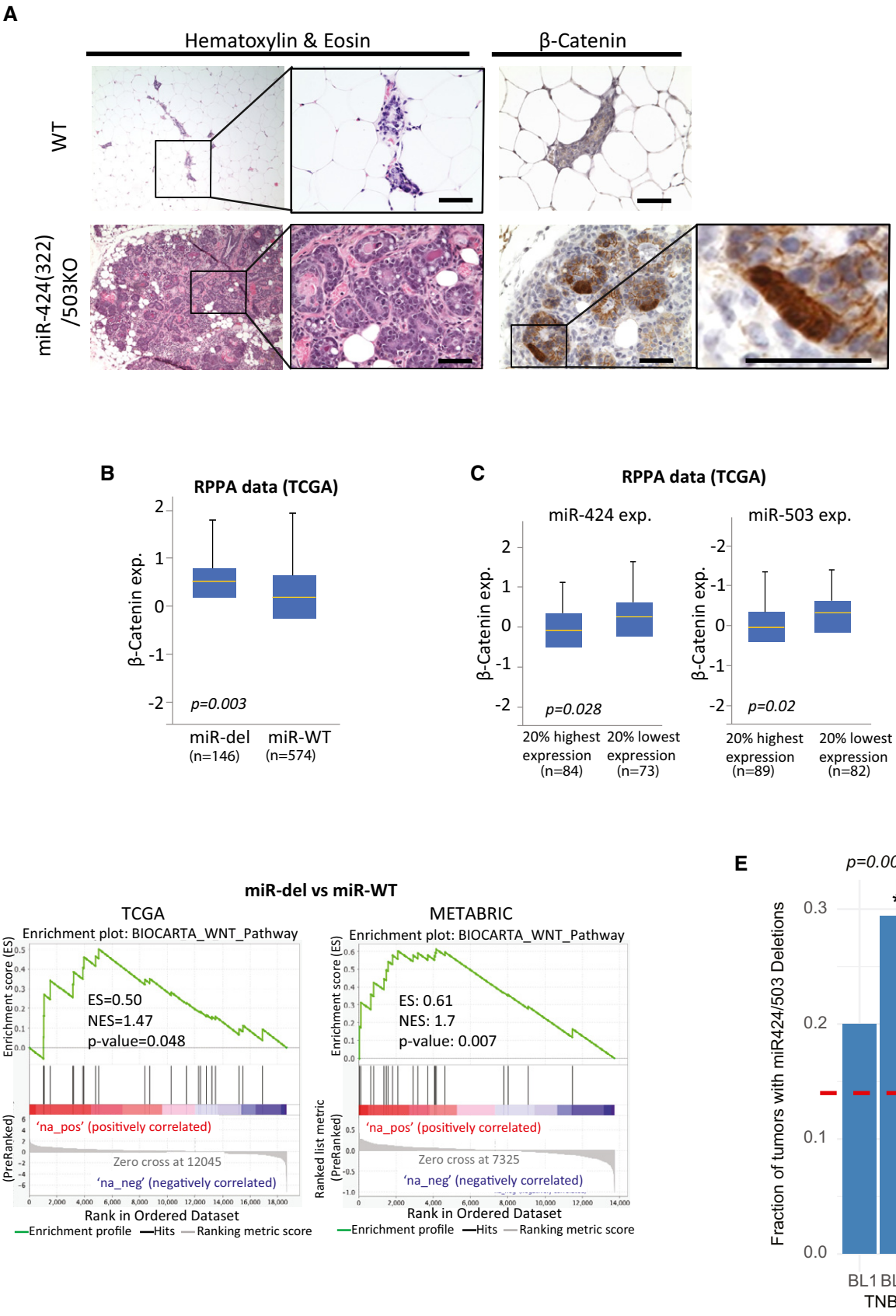
A
Hematoxylin & Eosin
β-Catenin
WT
miR-424(322)
/503KO
B
RPPA data (TCGA)
β-Catenin exp.
p=0.003
miR-del
(n=146)
miR-WT
(n=574)
C
RPPA data (TCGA)
miR-424 exp.
miR-503 exp.
β-Catenin exp.
p=0.028
p=0.02
20% highest expression
(n=84)
20% lowest expression
(n=73)
20% highest expression
(n=89)
20% lowest expression
(n=82)
D
miR-del vs miR-WT
TCGA
Enrichment plot: BIOCARTA_WNT_Pathway
ES=0.50
NES=1.47
p-value=0.048
'na_pos' (positively correlated)
Zero cross at 12045
'na_neg' (negatively correlated)
Enrichment score (ES)
Ranked list metric (PreRanked)
Rank in Ordered Dataset
Enrichment profile
Hits
Ranking metric score
METABRIC
Enrichment plot: BIOCARTA_WNT_Pathway
ES: 0.61
NES: 1.7
p-value: 0.007
'na_pos' (positively correlated)
Zero cross at 7325
'na_neg' (negatively correlated)
Rank in Ordered Dataset
Enrichment profile
Hits
Ranking metric score
E
p=0.00025
p=0.001
Fraction of tumors with miR424/503 Deletions
BL1
BL2
LAR
M
TNBC-subtype

Figure 1.

Figure 1. Loss of miR-424/503 is associated with tumors with elevated Wnt/β-catenin activity.

A H&E and immunohistochemistry reveal that β-catenin accumulates in tumors emerging in one-year-old female miR-424(322)/503$^{-/-}$ mice. The panel is a representative image of $n = 5$ independent tumors. The scale bar indicates 100 micrometers (μm).

B Bar graphic showing that human breast cancers with deletion of the miR-424/503 locus have higher protein levels of β-catenin (RPPA). *P*-value is calculated based on the one-sided Wilcoxon rank-sum test. In the boxplots in (B) and (C), the relative expression of β-catenin in the RPPA data from TCGA is shown. The yellow line indicates the median, and the bars indicate the 75th percentile (Q3)+1.5 interquartile range (IQR).

C The bar graph shows that human breast cancers with low expression levels of miR-424 and miR-503 have higher protein levels of β-catenin. *P*-value is calculated based on the one-sided Wilcoxon rank-sum test.

D GSEA indicating that tumors with deletion of the miR-424/503 locus present higher canonical Wnt signaling activity. Independent analysis for TCGA and METABRIC data sets are shown. *P*-values were obtained from the GSEA pipeline based on permutation tests.

E The graphic shows the enrichment of miR-424/503 deletions in the BL2 and M subtypes of TNBC. The red line shows the overall fraction of miR-424/503 deletions in TCGA samples. The enrichment in subtypes is estimated by the binomial test. The asterisks indicate the columns that the *P*-values above are linked to.

cells were separated by FACS into two main populations, basal (EpCAM^{low}CD49f^{hi}) and luminal (EpCAM^{high}CD49f^{low}) (Smalley *et al*, 2012). Luminal cells were further subdivided into hormone receptor positive and negative (HR$^{+/-}$) by Sca1 (Ly6a/e) levels, HR^{-} (EpCAM^{high}CD49f^{low}Sca-1^{-}) and HR^{+} (EpCAM^{high}CD49f^{low}Sca-1^{+}) (Smalley *et al*, 2012). Finally, a population enriched in MaSCs was purified from the basal compartment by PROCR expression, MaSC EpCAM^{low}CD49f^{high}PROCR^{+} (Wang *et al*, 2015). Remarkably, the expression of miR-424(322) and miR-503 was found to be more than 20-fold higher in MaSCs than in any other subpopulation during the estrus phase. However, during the expansion phase of the epithelium (diestrus), their expression was strongly reduced (Fig 2A).

Based on the high level of expression of miR-424(322)/503 in MaSCs and its association with Wnt signaling, we reasoned that its loss may impact the number of MaSCs in the mammary gland. Thus, we compared the amount of MaSCs present in WT and KO animals using two strategies. First, we compared the number of PROCR^{+} (MaSC enriched) using FACS. Remarkably, we found that old KO female mice (> 1 year) present ~ 2.5-fold increase in the total number of PROCR+ cells in the epithelial population (Fig 2B). FACS-based strategies to obtain MaSCs only render enriched populations. Thus, we also compared the number of MaSCs by using a functional assay. For this, we performed a mammary organoid assay (Zhang *et al*, 2016). This assay is based on the ability of MaSC and luminal precursors to form colonies when grown in Matrigel suspension and functions as a surrogate marker of the number of MaSCs with repopulation ability. Here, we observed that basal-containing MaSCs (EpCAM^{low}CD49f^{high}) from KO mice that were FACS-purified and grown in this assay consistently formed more organoids than those from age- and stage-matched WT cells (Fig 2C). As expected, the increased ability to form organoids was maintained when primary structures were disaggregated and plated again to form secondary organoids (Fig EV2). Finally, the number of luminal precursors forming colonies observed when luminal (EpCAM-^{highCD49flow}) cells were plated did not significantly change between WT and KO cells, indicating that the absence of miR-424(322)/503 is MaSC-specific (Fig 2C). All studies were performed using females during diestrus because it is well known that there are more MaSCs than during the estrus phase (Joshi *et al*, 2010).

Next, we transitioned our studies to a tractable model where miR cluster expression and WNT/β-catenin activation could be fully controlled, miR-cluster-Dox-MCF-10A (Llobet-Navas *et al*, 2014a.b). This is an in vitro model where the expression of miR-424/503 can be experimentally increased at will by using a doxycycline (Dox)-inducible system in human basal MCF-10A cells. Additionally, these cells accumulate nuclear β-catenin and upregulate Wnt-responsive genes upon the addition of WNT ligands (Fig 2D and E). Notably, upon upregulation of miR-424/503, both the accumulation of β-catenin and the upregulation of Wnt targets induced by adding WNT3a ligand into the culture media were strongly reduced (Fig 2D and E). This result confirms that miR-424/503 expression has a role in modulating canonical Wnt signaling.

miR-424(322)/503 modulates the expression of the Wnt co-receptor LRP6

MicroRNAs are small non-coding RNAs (20–22 nucleotides) that exert their function by interacting with targeted mRNAs, generally at the 3'UTR, through their seed sequence and reducing their overall expression by multiple mechanisms (Grimson *et al*, 2007). Thus, to explain the impact of miR-424/503 on WNT/β-catenin signaling, we hypothesized that one or more of its targets are components of this pathway. Computational prediction of targets based on seed sequence conservation and non-conserved sites is a widely used strategy to identify miRNA targets. We used the TargetScan algorithm (http://www.targetscan.org), which has been shown to have one of the highest specificities in preselecting putative target genes (Shirdel *et al*, 2011). Notably, TargetScan identified several components that positively regulate the canonical Wnt pathway and that could explain its activation upon miR-424/503 loss. These putative targets include Wnt ligands, receptors, and proteins associated with signal transduction. In fact, two of these, *LRP6* and *TBL1XRL*, were in the top 10% of the list when the putative targets were ordered based on their probability of conserved targeting score (PCT) (Fig 3A).

As MaSC cells are sensor cells that react to Wnt ligands, we decided to focus our studies on signaling components. Thus, we investigated the top two predicted putative targets, *Lrp6* and *TBL1XRL*, which contain 2 and 3 conserved binding sites, respectively (Figs 3A and B, and EV3A). To investigate whether these putative target genes are regulated by miR-424(322)/503, we first utilized a reporter system measuring the capacity of each predicted binding site to regulate gene expression upon experimental upregulation of miR-424 and miR-503 microRNAs. We then cloned a portion of the gene 3'UTR containing the predicted wild-type binding site downstream of a luciferase reporter gene. Next, we co-transduced 293T cells with the corresponding Luc-UTR reporter, a Renilla luciferase expression vector lacking any UTR, and used for

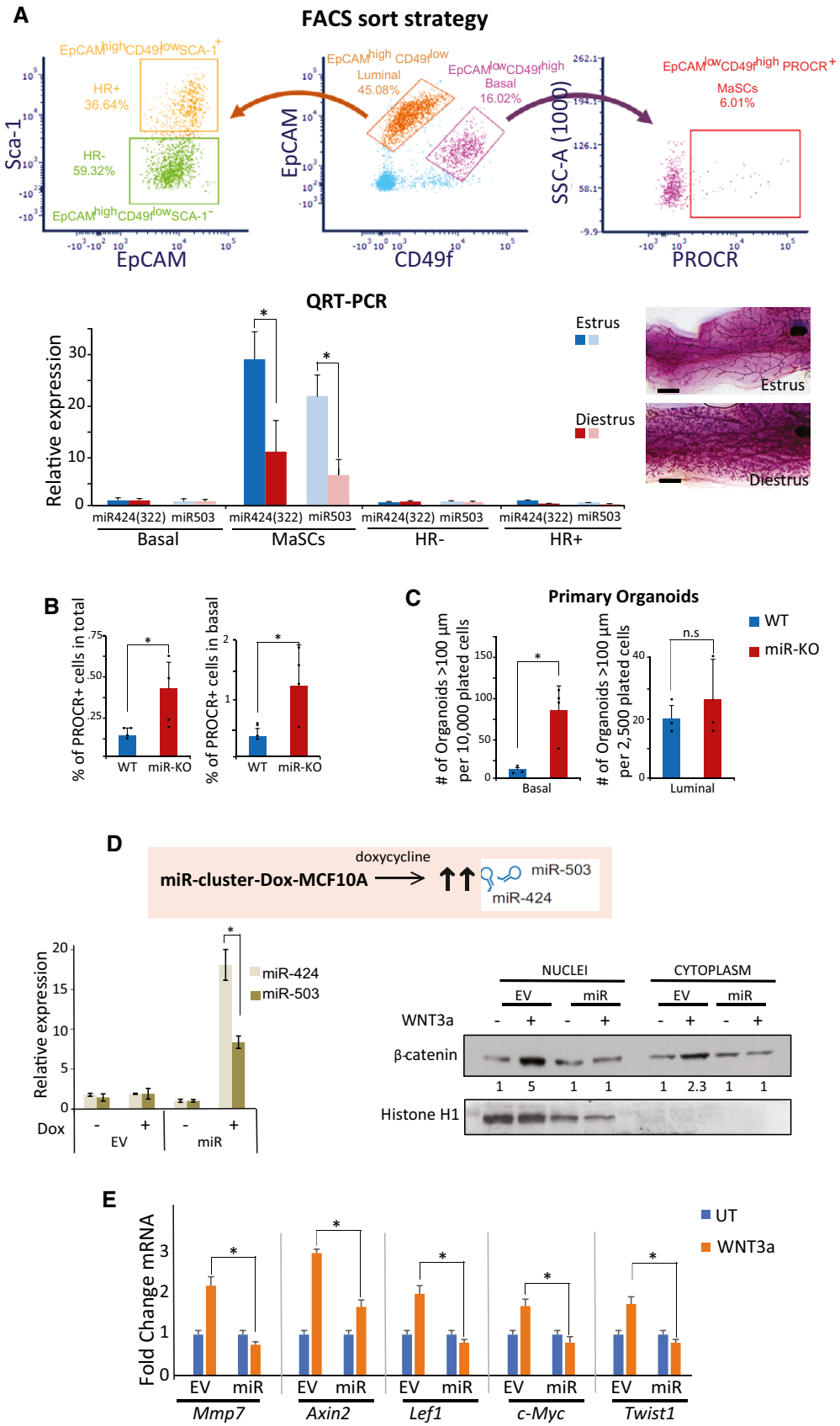
A
FACS sort strategy
EpCAMhighCD49flowSCA-1+
HR+
36.64%
HR-
59.32%
EpCAMhighCD49flowSCA-1-
Sca-1
EpCAM
EpCAMhigh CD49flow
Luminal
45.08%
EpCAMlowCD49fhigh
Basal
16.02%
CD49f
SSC-A (1000)
EpCAMlowCD49fhigh PROCR+
MaSCs
6.01%
PROCR
QRT-PCR
Relative expression
miR424(322) miR503
Basal
MaSCs
HR-
HR+
Estrus
Diestrus
B
% of PROCR+ cells in total
% of PROCR+ cells in basal
WT
miR-KO
C
Primary Organoids
# of Organoids >100 µm per 10,000 plated cells
# of Organoids >100 µm per 2,500 plated cells
Basal
Luminal
n.s
WT
miR-KO
D
doxycycline
miR-cluster-Dox-MCF10A
miR-503
miR-424
Relative expression
miR-424
miR-503
Dox
EV
miR
NUCLEI
CYTOPLASM
WNT3a
β-catenin
Histone H1
E
Fold Change mRNA
UT
WNT3a
Mmp7
Axin2
Lef1
c-Myc
Twist1

Figure 2.

Figure 2. Expression level of miR-424(322)/503 regulates Wnt/β-catenin activity.

A The upper panel indicates the FACS strategy followed to purify the different mammary epithelial subpopulations found in the mouse mammary gland (basal, luminal HR^{-}, luminal HR^{+}, and MaSCs). The lower panel shows the normalized expression of miR-424(503) and miR-503 revealing that MaSCs express the highest levels. The error bars show the standard deviation. FACS was performed at two different stages of the ovarian cycle (estrus and diestrus). Carmine-red staining of the structure of the mammary tree at the time of purification is also provided. The scale bar indicates 5 millimeters (mm).

B The bar graphs show the number of $PROCR^{+}$ in 1-year-old female WT and miR-424(322)/503 KO mice during diestrus. The error bars show the standard deviation.

C The bar graphs indicate the number of primary organoids formed when FACS-sorted WT or miR-424(322)/503 mammary epithelial basal and luminal cells from female mice at diestrus (4–6 months old) phase were cultured as organoids. The error bars show the standard deviation.

D The Western blot shows the difference in nuclear accumulation of β-catenin when dox-induced (100 ng/ml for 3 days) miR-cluster-Dox-MCF-10A cells (miR) and miR-control-Dox-MCF-10A cells (EV, empty vector) were exposed to WNT3a ligand (100 ng/ml for 6 h). The numbers below the blots indicate the quantitation by densitometry of protein expression relative to EV without WNT3A. Histone H1 staining is shown to control for nuclear–cytosolic purification. The upregulation of miR-424 and miR-503 when dox was added to the media was quantified by qRT–PCR and is shown in the bar graph. The error bars show the standard deviation.

E The panel shows the lack of induction of bona fide WNT targets in miR-overexpressing cells from panel (C) compared with EV control. UT indicates samples untreated with WNT3.

Data information: For all panels, the results shown are the average of $n \geq 3$ or representative images of $n \geq 3$ independent biological experiments. The asterisks indicate a P-value < 0.05 calculated by the t-test, and the bars show the standard deviation; n.s indicates no significant difference.
Source data are available online for this figure.

normalization purposes, and microRNA mimics corresponding to miR-424(322) and miR-503. Twenty-four hours after transfection, we quantified the expression of the Luc reporter (Fig 3B). These experiments revealed that miR-424 and miR-503 were able to significantly attenuate the expression of Luc when both conserved sites in *LRP6* and 2 out of the 3 conserved sites in *TBL1XR1* were cloned in the 3'UTR. The reduction in Luc expression was equivalent to the reduction observed in the positive control (CDC25A-binding site) (Fig 3B). In contrast, none of the non-conserved sites showed any effect. We also cloned the binding sites, conserved and non-conserved, from *GSKIP*, a predicted target that had a much lower PCT value. Notably, none of its biding sites had any effect on the expression of the reporter (Fig 3B). To finally demonstrate that the reduction in reporter expression was mediated by the interaction between the miRNA and the targeted mRNA, we mutated the sequences complementary to the miRNA's seed sequence (Grimson *et al*, 2007) to disrupt microRNA binding. As expected, this completely abrogated any reduction in reporter expression (Fig 3C).

Next, we tested whether the miR-424/503 can modulate the endogenous levels of LRP6 and TBLR1. First, we used the miR-cluster-Dox-MCF-10A model. Here, upon dox induction of the microRNA cluster, Western blot studies showed a clear downregulation in LRP6 protein, while a smaller effect was observed for TBLR1 (Fig 3D). As mentioned above, microRNAs exert their inhibitory function by multiple mechanisms. Some of these are associated with reduction of the mRNA level of targeted genes (e.g., mRNA decay) (Grimson *et al*, 2007; Eichhorn *et al*, 2014), and consequently, target downregulation can be investigated by qRT–PCR. Notably, we observed the reduction of the total level of *Lrp6* mRNA upon upregulation of the miR cluster (Fig EV3B). As expected, independent transduction of miR-424 and miR-503 mimics in MCF-10A cells showed that both can downregulate LRP6 (Fig EV3C). To complement our studies, we also performed loss of function in MCF-10A cells. For this, we blocked miRNA-424/503 with the introduction of miRNA hairpin inhibitors into cells. In agreement with the gain-of-function studies, we observed a clear upregulation of LRP6, while almost no effect was found for TBLR1 (Fig 3E). Next, we compared the expression of these putative targets in WT and KO basal-derived organoids in the presence or absence of WNT3a ligand. Again, KO cells showed higher basal expression levels of LRP6 than the WT counterpart, while no main differences were observed for TLBR1 (Fig 3F). Overall, these results support that miR-424/503 modulates LRP6 expression, but not TLBR1. Thus, next, we analyzed the expression of LRP6 in vivo in WT and miR cluster KO mammary glands by IHC. As expected, a clear upregulation of LRP6 was observed in the lesions found in the mammary epithelium of KO females (Fig 3G). To complement our studies, we evaluated the expression of *Lrp6* in FACS-purified $PROCR^{+}$ cells at early time points before tumor formation (4–6 months). qRT–PCR analysis revealed that miR cluster KO cells present a statistically significant increase in *Lrp6* mRNA levels (Fig EV3D). Finally, we wondered whether differential expression of LRP6 could be detected in breast cancer samples depending on the status of the miR-424/503 locus. Because there are not RPPA data available for LRP6 in TCGA data set, we investigated this question by analyzing the correlation between deletion of the miR-424/503 locus and expression of *Lrp6* mRNA. Here, again we observed breast cancer tumors with deletion of the miR cluster have a statistically significant increase in *Lrp6* mRNA levels (Fig EV3E).

Regulation of LRP6 by miR-424/503 is mediated by two conserved miRNA binding sites in the *Lrp6* mRNA 3' UTR

MicroRNAs downregulate the expression of targeted genes by recruiting mRNAs to the RNA-induced silencing complex (RISC) (Grimson *et al*, 2007). To further investigate the regulation of miR-424/503 on LRP6 expression, we performed additional studies using PAR-CLIP of mRNAs bound to RISC (Hafner *et al*, 2010). Briefly, this is a biochemical assay where the RISC complex and the mRNAs being targeted are immunoprecipitated (IP) using antibodies for the RISC component AGO2. The amount of a particular mRNA bound to RISC is enriched in the IP when a microRNA that modulates its expression is experimentally upregulated. Additionally, the enrichment of RISC in a particular binding site can be determined by simple qRT–PCR. Here, we observed a significant enrichment of *LRP6* mRNA bound to RISC, specifically at the binding site#1, when the miR cluster was induced in the miR-cluster-Dox-MCF-10A model (Fig 4A). To investigate the contribution of the #1 and #3 binding sites in *Lrp6*, we used a strategy called target protection. In brief,

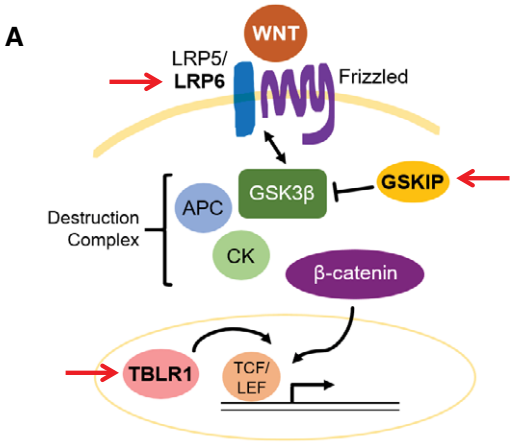

Gene	Predicted Human miR-424 target	Conserved sites	Poorly conserved sites
LRP6	(top10%)	2	1
TBLR1	(top10%)	3	1
GSKIP	(below 60%)	1	2
CTNNBIP1	(below 60%)	1	0
WIF	(below 80%)	1	0

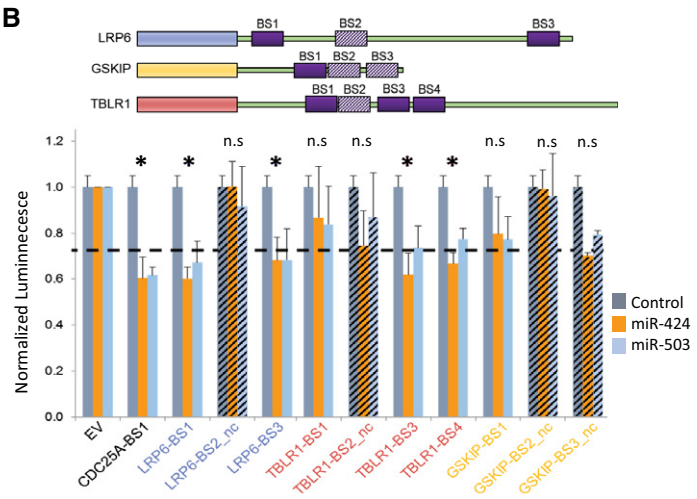

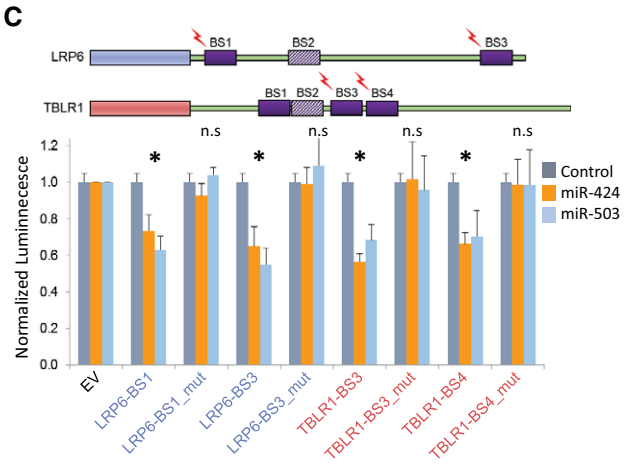

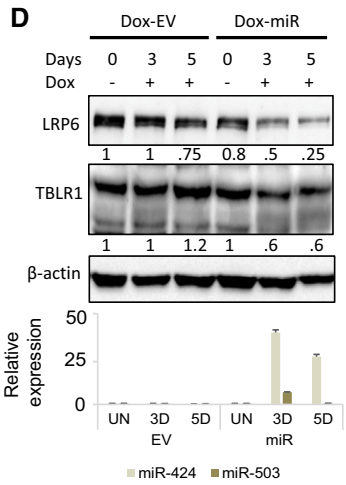

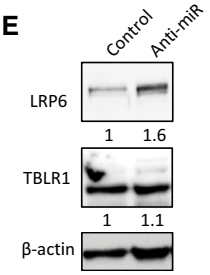

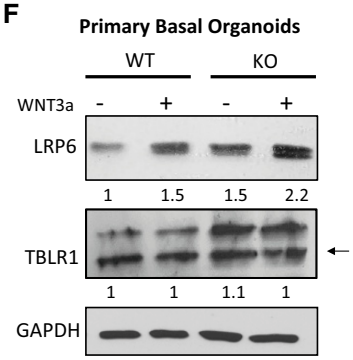

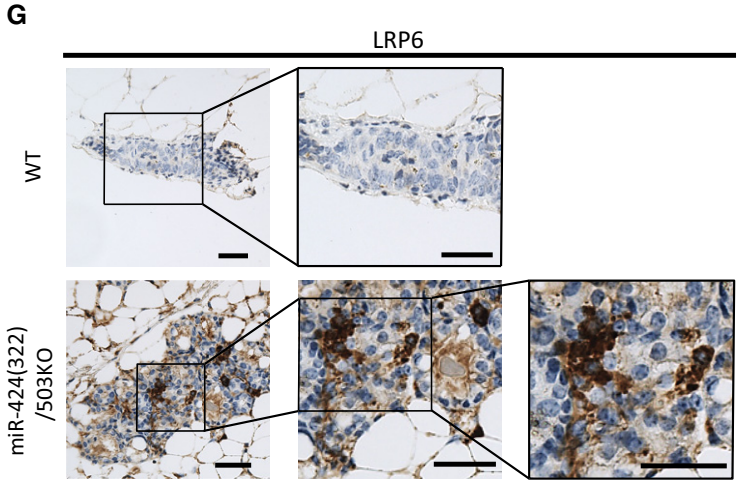

Figure 3.

Figure 3. miR-424/503 cluster targets the Wnt co-receptor LRP6.

A The table shows putative miR-424(322)/503 targets selected from the TargetScan database and ranked based on their probability of conserved targeting. A schematic representation of the canonical Wnt pathway with arrows indicating the putative targets that were investigated is also shown.

B The upper panel illustrates the location of the conserved and non-conserved (-nc) predicted microRNA binding sites in the 3'UTR of 3 selected target genes. The bar graph compares the normalized expression of a firefly luciferase reporter (luc) plasmid (EV) after transfection in 293T cells and the same luc reporter with a modified 3'UTR containing predicted microRNA binding sites. The values represent the ratio of luc expression when the reporter was co-transfected with synthetic miR-424 and miR-503 vs. a control non-targeting sequence. The bars with a diagonal line pattern indicate non-conserved sites. A known miR-424/503 binding site located in the 3'UTR of CDC25 is used as a positive control. The horizontal line indicates 25% of reduction in luminescence, and it is included as a visual reference. The error bars show the standard deviation.

C Luciferase assays showing that the effect of the miR-424 and miR-503 on luc expression is abrogated when the seed sequence in the microRNA binding sites was mutated. The study was performed in four sites statistically significant from panel (B). The error bars show the standard deviation.

D Western blot of LRP6 and TBLR1 in the miR-cluster-Dox-MCF-10A model upon upregulation of miR cluster with 100 ng/ml of doxycycline for the specified number of days. The numbers below the blots indicate the quantitation by densitometry of protein expression relative to β-actin. The expression level of miR-424 and miR-503 is indicated in the bar graph below the blots. UN indicates samples untreated with doxycycline. The error bars show the standard deviation.

E Western blots of LRP6 and TBLR1 in parental MCF-10A cells after transfection with miRNA hairpin inhibitors against miR-424/503.

F Western blot of LRP6 and TBLR1 expression in WT and miR-424/503 KO basal cell-derived organoids after 14 days in culture with and without Wnt3a (100 ng/ml). The arrow shows the correct TBLR1 band.

G IHC staining showing that LRP6 accumulates in the epithelium of female miR-424(322)/503$^{-/-}$ mice (1-year-old). The scale bar indicates 100 micrometers (μm).

Data information: For all panels, the results shown are the average of $n \geq 3$ or representative images of $n \geq 3$ independent biological experiments. The asterisks indicate a P-value < 0.05 calculated by the t-test, and the bars show the standard deviation; n.s indicates no significant difference. The numbers under the blot indicate the quantification of the bands done by densitometry.
Source data are available online for this figure.

the expression of a short 60mer RNA that is complementary to the region that contains the binding site in the mRNA 3'UTR protects the binding site from the microRNA and prevents target inhibition (Knauss *et al*, 2013; Yongblah *et al*, 2018). As expected, blockage of both sites completely prevented the reduction of LRP6 protein upon upregulation of miR-424/503 in the miR-cluster-Dox-MCF-10A model (Fig 4B). Interestingly, blocking the binding site#1 had the most pronounced effect of the two when blocked individually (Fig 4B).

Next, we took advantage of the target protection strategy to investigate the impact that blocking the interaction between the miR cluster and Lrp6 mRNA has on the response to WNT ligands. For this, we studied the expression of β-catenin in miR-cluster-Dox-MCF-10A cells that overexpress the miR cluster (Dox in the culture media) and are exposed to WNT3 ligand after the microRNA binding sites were blocked by target protection. Here, protection of the conserved #1 and #3 microRNA binding sites prevented the downregulation of LRP6 and allowed the accumulation of β-catenin (Fig 4C).

Regulation of mammary epithelial dynamics by miR-424(322)/503

Overall, our study shows that miR-424(322)/503 expression influences canonical Wnt signaling in the mammary epithelium and that its loss promotes upregulation of the WNT/β-catenin signaling. How does this miR cluster exert this function? Our data provide compelling evidence that miR-424(322)/503 directly binds to the 3'UTR of the *Lrp6* mRNA, the co-receptor for Wnt ligands, and that this binding attenuates LRP6 expression. There are three putative binding sites for this cluster located at the *Lrp6* 3'UTR (Fig EV3A). We demonstrate here that sites #1 and #3 but not #2 are able to modulate protein expression in concert with miR-424(322)/503. Remarkably, #1 and #3 sites are conserved through evolution while site #2 is not, which highlights the importance of these binding sequences. It is worth mentioning that although functional 3'UTR luciferase assays indicate that both conserve sites are active (Fig 3B and C), PAR-CLIP and target protection studies show that they are not fully equivalent and that the #1 site is the most potent (Fig 4A and B). *Lrp6* is not the only gene associated with Wnt signaling that is predicted to be a target of miR-424(322)/503, and here, we have investigated two of the other top predicted candidates, *Tblr1* and *Gskip*. Although we have not been able to demonstrate that they are robust targets in the mammary epithelium, they may be relevant in other biological contexts. Nonetheless, as LRP6 is a rate-limiting factor of the WNT/β-catenin pathway (Brennan & Brown, 2004) LRP6 is likely the most significant miR-424(322)/503 target for WNT pathway regulation.

We and others have previously shown that miR-424/503 targets genes such as *IGF1R* and *BCL2* in the mammary epithelium and that its loss affects developmental processes (involution) and tumorigenesis (Llobet-Navas *et al*, 2014a; Rodriguez-Barrueco *et al*, 2017; Mertelmeyer *et al*, 2020). The newly discovered regulation of WNT signaling presents a clearer and more complete view of the function of this microRNA cluster modulating mammary epithelial fate. Thus, to integrate our novel and previous results with the current understanding of mammary gland development and cancer we propose the following model (Fig EV4). During regular ovarian cycles, at the diestrus phase, there is an increase in the mammary epithelial content of the mammary gland, the purpose of which is to prepare the mammary gland for a potential pregnancy. If pregnancy occurs, gland remodeling becomes widespread (Macias & Hinck, 2012). Expansion of the mammary epithelium during diestrus and pregnancy is mediated by a profound and transient increase in the MaSC pool (Asselin-Labat *et al*, 2010; Joshi *et al*, 2010; van Amerongen *et al*, 2012). This is due to the activation of Wnt/β-catenin signaling in MaSCs responding to RANK and WNT ligands secreted from luminal/HR+ cells (Alexander *et al*, 2012; Goel *et al*, 2012). After expansion, the mammary epithelium involutes to return to its original state; this process includes the reduction in the number of MaSCs (Asselin-Labat *et al*, 2010). As shown here, during periods of epithelial expansion (e.g., diestrus), miR-424(322)/503 is reduced in MaSCs to promote Wnt/β-catenin signaling. During

periods of epithelial regression, miR-424(322)/503 upregulation in luminal and basal cells attenuates BCL2 and IGF1R expression inducing cell death/apoptosis (Llobet-Navas *et al*, 2014a; Rodriguez-Barrueco *et al*, 2017) and, as our data indicate, reducing Wnt/β-catenin signaling in MaSCs by targeting LRP6. The loss of miR-424(322)/503 in breast cancers (Rodriguez-Barrueco *et al*, 2017) and miR KO mice sensitizes MaSCs to WNT stimuli during phases of epithelial expansion and promotes aberrant survival of mammary epithelial cells due to upregulation of BCL2 and IGF1R during periods of epithelial regression. This accumulates through

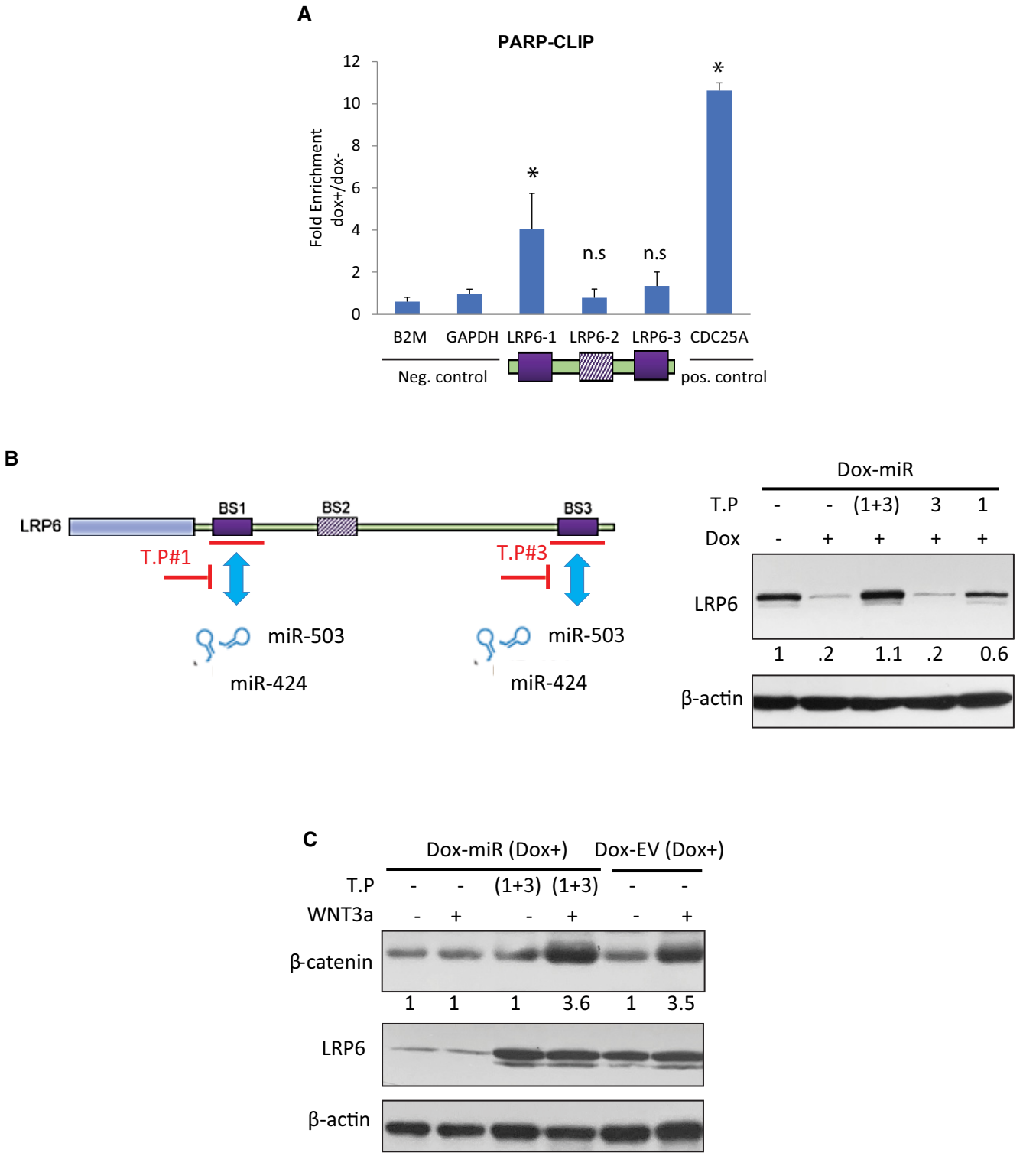

Figure 4.

Figure 4. Regulation of LRP6 by miR-424/503 occurs through the *Lrp6* mRNA 3' UTR.

A Enrichment of the putative LRP6 binding sites bound to AGO2 in miR-cluster-Dox-MCF-10A cells after the miR-424/503 cluster is induced with 100 ng/ml of dox for three days. A CDC25A-binding site is included as a positive control, and a region of B2M and GAPDH are included as negative controls. The error bars show the standard deviation.

B The WT blot shows the expression of LRP6 upon upregulation of miR-424/503 in miR-cluster-Dox-MCF-10A cells (Dox^+) when one or both of the conserved microRNA binding sites (#1 and #3) are blocked by target protection.

C The WT blot shows the expression of LRP6 and β-catenin in cells in miR-cluster-Dox-MCF-10A cells cultured in the presence of Dox and with and without WNT3a ligand (100 ng/ml for 6 h) when the microRNA binding sites #1 and #3 are blocked by target protection.

Data information: For all panels, the results shown are the average of $n \geq 3$ or representative images of $n \geq 3$ independent biological experiments. The asterisks indicate a P-value < 0.05 calculated by the t-test, and the bars show the standard deviation; n.s indicates no significant difference. The numbers under the blot indicate the quantification of the bands done by densitometry.
Source data are available online for this figure.

the female lifetime promoting tumorigenesis (Rodriguez-Barrueco *et al*, 2017).

Finally, an important finding of our study is the high level of miR-424/503 deletions in TNBCs of the BL2 and M subtypes. It has been long recognized that Wnt signaling is activated in some breast cancers, especially in the TNBC group (Lehmann *et al*, 2011). However, the molecular alterations linked to it have remained elusive. Thus, our study has unveiled a molecular alteration that can explain a large fraction (~ 25%) of all cases.

Our studies have some limitations that are worth discussing. We have shown that loss of the miR cluster increases the number of MaSCs in the mammary gland, and the ability to form organoids. But what does induce this phenotype? As mention above, miR-424/503 influences cell proliferation by directly regulating CDC25, BCL2, and IGF1R. Additionally, activation of Wnt signaling induces c-Myc, which is a master regulator of cell division. Consequently, loss of miR-424/503 influences multiple pathways, being Wnt signaling one of them, which affects proliferation. Thus, this is likely to be relevant, but not the only one, for the observed increase in MaSCs. Defining what is the precise contribution of each of the pathways to the observed phenotype is out of the scope of this manuscript and will require additional investigation.

In summary, the results presented here unveil an unknown link between the miR-424/503, the regulation of WNT signaling, MaSC fate, and tumorigenesis.

Materials and Methods

Animal models

The generation of miR-424(322)/$503^{-/-}$ animals has been previously described (Llobet-Navas *et al*, 2014a; Rodriguez-Barrueco *et al*, 2017). All animal studies described here have been approved by the corresponding institutional IACUC.

Patient data analysis

Patient data from TCGA-BRCA (Cancer Genome Atlas, 2012) consist of breast cancer samples with available whole-genome DNA copy-number alterations, mRNA expression data, and clinicopathological and reverse-phase protein array (RPPA) data. Patient data from METABRIC (Curtis *et al*, 2012) were analyzed for whole-genome DNA copy-number alterations and mRNA expression data.

Cell culture

Cell lines were obtained from the American Type Culture Collection (ATCC). MCF-10A cells were cultured in DMEM/Ham's F12 media supplemented with 1% penicillin–streptomycin, EGF (20 ng/ml), insulin (10 μg/ml), cholera toxin (100 ng/ml), hydrocortisone (500 ng/ml), and 5% horse serum. We cultured 293T cells in DMEM with 1% penicillin–streptomycin and 10% FBS. In some cases, described in the text, Wnt3a ligand (R&D Systems 5036-WN) at 100 ng/ml was added to the culture. MiRNA inhibition in MCF-10A cells was achieved by transducing cells with a miRNA inhibitor against hsa-miR-424-5p and hsa-miR-503-5p (GeneCopoeia #HmiR-AN0494-AM03 and #HmiR-AN0550-AM03, respectively). Control cells were generated by transducing a scrambled control (GeneCopoeia #CMIR-AN0001-AM039).

miR-cluster-Dox-MCF-10A

The generation of these cells has been previously described (Llobet-Navas *et al*, 2014a; Rodriguez-Barrueco *et al*, 2017). Doxycycline was added to the media at 100 ng/ml to induce the expression of miR-424/503.

RNA and protein analysis

To perform microRNA expression analysis by qRT–PCR, RNA was extracted using the mirVana miRNA isolation Kit (Ambion #AM1561) according to the manufacturer's instructions. Reverse transcription and qPCR were performed according to the TaqMan microRNA Assay protocol and as previously described using probes for murine miR-322, miR-503, and snoRNA-202 (Thermo Fisher #001076, 002456, and 001232, respectively). The thermal cycler conditions were as follows: activation at 95°C for 10 min, denaturation at 95°C for 15 s, and annealing/extension at 60°C for 1 min (repeated for 40 cycles). Ct values (2-ΔΔCT) were calculated by normalizing to an endogenous reference gene (snoRNA-202). To assess the expression of Wnt/ β-catenin target genes, total RNA was converted into cDNA using the High-Capacity cDNA Reverse Transcription Kit (Roche #4368814) according to the manufacturer's instructions. Two microliters of the reverse transcription reaction was used as a template for real-time detection on a Bio-Rad MyiQ Single-Color Real-Time PCR Detection System. For coding genes, the real-time PCR was performed with 10 μl FastStart SYBR Green Master Mix (Roche #04673492001), 2 μl of complementary DNA

(cDNA), and 1 μl of each primer in RNase-free water adjusted to 20 μl volume reaction. The following were the thermal cycler conditions: AmpliTaq activation at 95°C for 3 min, denaturation at 95°C for 10 s, and annealing/extension at 60°C for 30 s (repeat 40 times). Triplicate Ct values were further analyzed (2-ΔΔCT) by normalizing to an endogenous reference gene (GAPDH). Results are presented as the relative mRNA amount compared with the untreated samples. Primers used were as follows: *GAPDH* (F CATCTTCTTTTGCGTCGC, R AAAAGCAGCCCTGGTGAC); *MMP7* (F GAGTGAGCTACAGTGG GAACA, R CTATGACGCGGGAGTTTAACAT); *AXIN2* (F CAACAC CAGGCGGAACGAA, GCCCAATAAGGAGTGTAAGGACT); *LEF1* (FAGAACACCCCGATGACGGA, R GGCATCATTATGTACCCGGA AT); *MYC* (F TCCCTCCACTCGGAAGGAC, CTGGTGCATTTTCG GTTGTTG); and *TWIST1* (F GTCCGCAGTCTTACGAGGAG, R GCTTGAGGGTCTGAATCTTGCT).

qRT–PCR for mouse miR-424(322) and miR-503 was performed using TaqMan microRNA probes (Thermo Fisher# 001076, # Mm04238302s1). qRT–PCR for human miR-424(322) and miR-503 was performed using SYBR Green as described in Llobet *et al* Genes Dev. 2014 Apr 1;28(7):765–782.

Western blotting

Cells were lysed in RIPA buffer with 30 mM NaF, 1 mM Na3VO4, 40 mM β-glycerophosphate, 0.1 mM PMSF, and protease inhibitors. Protein concentrations were determined by the Protein Assay Kit (Bio-Rad #500-0006). We subjected equal amounts of proteins to SDS–PAGE and transferred them to nitrocellulose membranes (GE Healthcare #10401197). Non-specific binding was blocked by incubation with TBST plus 5% non-fat milk. We incubated the membranes with primary antibodies overnight at 4°C and with secondary HRP-conjugated antibodies (Amersham #NA9350V, #NA931V, and #NA934V) for 1 h at room temperature. Signal was detected with SuperSignal West Pico or Dura Extended Duration Chemiluminescent Substrate (Thermo #34079 or #34076). The primary antibodies we used for these studies are as follows: anti-β-catenin (Abcam #ab2365), anti-LRP6 (Cell Signaling #3395), anti-TBLR1 (Bethyl Laboratories #A300-408A), and anti-GAPDH (Cell Signaling #14C10). Quantification of Western blot signal was performed using a ChemiDoc Imaging Systems and the Image Lab Software package (Bio-Rad).

Whole-mount preparations and immunohistochemistry

Mammary glands were fixed in formalin (Fisher #175) for immunohistochemistry (IHC) analysis. Whole-mount carmine red staining to visualize the mammary tree branching was prepared as follows: Mammary glands were dissected and fixed in paraformaldehyde 4% for 1 h. Afterward, samples were stained with carmine red (Sigma #C1022) overnight at room temperature. The next day, samples were dehydrated in increasing concentrations of ethanol (70%, 95%, and 100%) and ultimately fixed in xylene.

Formalin-fixed paraffin-embedded samples were first heated at 100°C for 3 min on a heat block to melt the paraffin. Subsequently, samples were deparaffinized by serial incubations with xylene for 3 min, 100% EtOH for 3 min, 95% EtOH for 3 min, and distilled water for 2 min. Peroxidase inactivation and antigen retrieval were achieved by incubating samples in 1% H_2O_2 for 15 min at room temperature and incubating slides with citric buffer (2 mM citric acid, 8 mM sodium citrate) in a steamer for 30 min. Samples were washed twice in PBS for 5 min and incubated in 10% whole goat blocking serum diluted in 2% BSA–PBS for 30 min at room temperature. Samples were then incubated in primary antibody diluted in 2% BSA–PBS+0.01% sodium azide for 2 h at room temperature. Antibodies were used at 1:300 anti-cytokeratin 18 antibody (Abcam #ab668) and 1:1,000 anti-cytokeratin 5 (Covance #PRB-160P). The remaining antibodies used were the same as for WT blotting but used at 1:100. Samples were then washed in PBS and incubated in 1:500 biotinylated anti-rabbit IgG made in goat diluted in 2% BSA–PBS for 30 min at room temperature. Afterward, samples were washed and exposed to peroxidase substrate (Vector Laboratories #PK-6100) for 30 min at room temperature and subsequently permeabilized with PBS–0.5% Triton. Thereafter, samples were incubated in chromogen 3,3'-diaminobenzidine (DAB) and then washed in distilled water and counterstained. Counterstaining was performed by treating samples with hematoxylin for 1 s, dipped in 1% hydrochloric acid, and finally washed in ammonia water for 1 s. Finally, dehydration was performed by incubating samples in 95% EtOH for 2 min, 100% EtOH for 2 min, and xylene for 4–5 min and ultimately mounted with a coverslip.

Nuclear fractionation

NF was performed using the NE-PER™ Nuclear and Cytoplasmic Extraction Reagents and following the instructions provided by the vendor (Life Technologies # 78833).

Luciferase reporter assays

To measure the targeting activity of miR-424(322)/503, we cloned oligonucleotides corresponding to the region of the 3'UTR containing each miRNA binding site (plus 30 bp upstream and downstream) downstream of the luciferase reporter in the pMIR-REPORT vector (Life Technologies #AM5795M) using restriction enzymes. For the mutagenesis, the same method was followed except that we randomly mutated the 8 base pair sequence corresponding to the miRNA seed sequence. To measure luciferase activity, 293T cells were seeded at 70% confluence in 96-well plates. 24 h later, we co-transfected the cells with 50 ng of pMIR-REPORT constructs containing the 3'UTR sequences together with 50 ng of a Renilla housekeeping control plasmid and 100 nM of miR-424 or miR-503 mimics or a miRNA negative control (Dharmacon #C-300717-05, #C-300841-05, or #CN-001000-01-05, respectively) using the TransIT-X2 reagent (Mirus 6003). 24 h after transfection, we measured the relative luciferase units (RLU) using the Dual-Glo Luciferase Assay System (Promega #E2949).

PAR-CLIP

The PAR-CLIP assay to measure the enrichment of miR-424(322)/503 mRNA targets bound to AGO2 was performed as described previously (Hafner *et al*, 2010). Briefly, cells were pretreated with 50 μM of 4-thiouridine (Sigma #T4509) overnight and crosslinked at 150 mJ/cm^2 at 365 nm UV on ice. Cells were reconstituted in lysis buffer [2.5 mM HEPES, pH 7, 50 mM NaCl, 10% glycerol, 1% Triton X-100, proteinase inhibitor (Roche #04693159001), 0.2 mM DTT, and 1 U/μl RNaseOUT (Invitrogen #10777-019)]. Mild (5 U/

μl) RNase-T1 (Fermentas #EN0541) digestion was performed at 22°C for 15 min. Immunoprecipitation was performed using A-beads (Roche #11719408001), G-beads (Roche #11719416001), and 10 μg of anti-AGO2 antibody (Abnova #H00027161-M01) overnight at 4°C. Samples were subsequently washed twice with washing buffer 1 (50 mM Tris, pH 7.5, 150 mM NaCl, 0.1% NP-40, and 1 mM EDTA) at 4°C for 30 min, digested with RNase-T1 (20 U/μl) at 22°C for 15 min, washed once with washing buffer 2 (50 mM Tris, pH 7.5, 500 mM NaCl, and 0.1% NP-40) at 4°C for 30 min, and finally washed twice with washing buffer 3 (50 mM Tris, pH 7.5, and 500 mM NP-40) at 4°C for 30 min. Samples were centrifuged for 5 min at 5,000 rpm at 4°C, and the supernatant was treated with 5 mg/ml of proteinase K (New England Biolabs #P8102) for 1 h at 50°C. Finally, the extract was lysed, and the RNA was extracted using the miRVana miRNA Isolation Kit (Ambion #AM1561) according to the instructions provided. Primer sequence used to measure LRP6 binding site (BS) enrichment in RISC by qRT–PCR was as follows: LRP6-BS1 (F TTTGTACAGAAGAAAAGGAT, R AGTTTGCAAAAATAAAACTT); LRP6-BS2 (F GAATAATGGAAGCC TCTTT, R CTAGAATCATTCCACAGGT); and LRP6-BS3 (F TACCAA GAAGATTAAACTGG, R AGATTAAAGCTTAAGGGAAA). Primers for negative/positive controls were as follows: GAPDH (F CATCTT CTTTTGCGTCGC, R AAAAGCAGCCCTGGTGAC); B2M (F TGCTGTCT CCATGTTTGATGTATCT, R TCTCTGCTCCCCACCTCTAAGT); and CDC25A (F GCCATTCTAGGTAGGGTTTT, R CCTAGCTTTCTGTCC GATAA).

Target protection

60mer RNAs complementary to the region in the 3'UTR of Lrp6 that contains the miR cluster binding site in the middle were transduced at a 100 nM final concentration in miR-cluster-Dox-MCF-10A cells. Transduction of these target protection sequences (TP) was done 24 h before induction of miR-424/503 with doxycycline and 96 h before addition of Wnt3a ligand (R&D Systems 5036-WN) at 100 ng/ml.

Mammary gland dissociation and FACS

The 3rd and 4th mammary glands from female mice of the specified age, genotype, and estrous cycle phase were pooled in PBS and minced followed by enzymatic digestion in DMEM/F12 media containing 2 mg/ml collagenase A (Roche #11088793001) and 100 U/ml hyaluronidase (Sigma #H3506) for 2 h at 37°C. Single-cell suspensions were obtained via sequential incubations in prewarmed 0.25% trypsin–EDTA followed by 5 mg/ml Dispase II (Life Technologies #17105-041) in PBS with 0.1 mg/ml DNase I (StemCell #07900), pipetting up and down at each step. Finally, cells were incubated in Red Blood Cell Lysing Buffer (Sigma #R7757) and filtered through a 40-μm cell strainer. Then, epithelial cells were obtained using the EasySep Mouse Epithelial Cell Enrichment Kit II (StemCell #19758) according to the protocol provided. The epithelial cell-enriched suspensions were incubated with the following antibodies: EpCAM-PerCP/Cy5.5, CD49f-APC, PROCR-PE, and Sca-1-BV421 (BioLegend #118220, #313616, #141504, and BD #562729, respectively) to sort the different epithelial subpopulations. To determine cell viability, we used the LIVE/DEAD™ Fixable Aqua Dead Cell Stain (Thermo Fisher #L34957). Antibody incubations were performed for 15 min on ice before sorting the cells using a FACSAria II cell sorter (BD).

Organoid culture

FACS-sorted cells were seeded into 24-well ultra-low attachment plates at a density of 5,000 or 10,000 cells/well in EpiCult-B Mouse Medium (StemCell #05610) supplemented with 5% FBS, 10 ng/ml EGF, 20 ng/ml bFGF, 4 μg/ml heparin, 5 μM Y-27632, and 5% Matrigel (Corning #354230). After 7 days in culture, the organoids were measured. For the generation of secondary organoids, the organoids were dissociated by incubating primary organoids in 0.25% trypsin–EDTA in PBS for 5 min at 37°C followed by mechanical disruption with a P1000 pipette. Finally, cells were filtered using a 40-μm cell strainer to ensure a single-cell suspension and seeded them again into 24-well ultra-low attachment plates, and the number of organoids > 100 μm in diameter after 7 days were counted as described above. In some cases, described in the text, Wnt3a ligand (R&D Systems 5036-WN) at 100 ng/ml was added to the culture.

Data availability

No large primary data sets have been generated and deposited.

Expanded View for this article is available online.

Acknowledgements
This study has been partially funded by the NY-state breast cancer grant program (Peter T. Roley) DOH01-ROWLY6-2021-00045-C36613GG (JS); the JGW-Patterson Foundation (30015.088.072PA/IXS); the Instituto de Salud Carlos III (ISCIII) through the projects CP17/00063 (cofounded by European Regional Development Fund (ERDF) "a way to build Europe") and MS17/00063 (co-founded by the European Social Fund (ESF), "investing in your future") (DLN); and the Ministerio de Ciencia, Innovación y Universidades Gobierno de España, through the projects RyC-2016-19671 and RTI2018-095611-A-I00 (RRB). The study was supported by the National Cancer Institute (NCI) of the National Institutes of Health (NIH) under award number F31CA232691 (EN). The data in this paper were used in a dissertation as partial fulfillment of the requirements for a Ph.D. degree at the Graduate School of Biomedical Sciences at Mount Sinai.

Author contributions
JS and DL-N conceived, designed, and supervised the research and wrote the manuscript. JS, DL-N, EAN, RR-B, MLD, and LD-J developed the experimental methodology. JY and K-KY coordinated and performed the computational analysis. EAN and RR-B had equal contributions coordinating and performing the wet laboratory studies described in the text. RLW and PM contributed to the animal studies. All authors contribute to data analysis and manuscript editing and wrote different parts of the Materials and Methods section.

Conflict of interest
The authors declare that they have no conflict of interest.

References

Alexander CM, Goel S, Fakhraldeen SA, Kim S (2012) Wnt signaling in mammary glands: plastic cell fates and combinatorial signaling. *Cold Spring Harb Perspect Biol* 4: a008037

van Amerongen R, Bowman AN, Nusse R (2012) Developmental stage and time dictate the fate of Wnt/beta-catenin-responsive stem cells in the mammary gland. *Cell Stem Cell* 11: 387 – 400

Asselin-Labat M-L, Vaillant F, Sheridan JM, Pal B, Wu DI, Simpson ER, Yasuda H, Smyth GK, Martin TJ, Lindeman GJ *et al* (2010) Control of mammary stem cell function by steroid hormone signalling. *Nature* 465: 798 – 802

Brennan KR, Brown AM (2004) Wnt proteins in mammary development and cancer. *J Mammary Gland Biol Neoplasia* 9: 119 – 131

Cancer Genome Atlas N (2012) Comprehensive molecular portraits of human breast tumours. *Nature* 490: 61 – 70

Curtis C, Shah SP, Chin S-F, Turashvili G, Rueda OM, Dunning MJ, Speed D, Lynch AG, Samarajiwa S, Yuan Y *et al* (2012) The genomic and transcriptomic architecture of 2,000 breast tumours reveals novel subgroups. *Nature* 486: 346 – 352

Diaz-Guerra E, Lillo MA, Santamaria S, Garcia-Sanz JA (2012) Intrinsic cues and hormones control mouse mammary epithelial tree size. *FASEB J* 26: 3844 – 3853

Eichhorn SW, Guo H, McGeary SE, Rodriguez-Mias RA, Shin C, Baek D, Hsu SH, Ghoshal K, Villen J, Bartel DP (2014) mRNA destabilization is the dominant effect of mammalian microRNAs by the time substantial repression ensues. *Mol Cell* 56: 104 – 115

Fernandez-Valdivia R, Mukherjee A, Ying Y, Li J, Paquet M, DeMayo FJ, Lydon JP (2009) The RANKL signaling axis is sufficient to elicit ductal side-branching and alveologenesis in the mammary gland of the virgin mouse. *Dev Biol* 328: 127 – 139

Goel S, Chin EN, Fakhraldeen SA, Berry SM, Beebe DJ, Alexander CM (2012) Both LRP5 and LRP6 receptors are required to respond to physiological Wnt ligands in mammary epithelial cells and fibroblasts. *J Biol Chem* 287: 16454 – 16466

Grimson A, Farh KK, Johnston WK, Garrett-Engele P, Lim LP, Bartel DP (2007) MicroRNA targeting specificity in mammals: determinants beyond seed pairing. *Mol Cell* 27: 91 – 105

Hafner M, Landthaler M, Burger L, Khorshid M, Hausser J, Berninger P, Rothballer A, Ascano M, Jungkamp A-C, Munschauer M *et al* (2010) Transcriptome-wide identification of RNA-binding protein and microRNA target sites by PAR-CLIP. *Cell* 141: 129 – 141

Joshi PA, Jackson HW, Beristain AG, Di Grappa MA, Mote PA, Clarke CL, Stingl J, Waterhouse PD, Khokha R (2010) Progesterone induces adult mammary stem cell expansion. *Nature* 465: 803 – 807

Knauss JL, Bian S, Sun T (2013) Plasmid-based target protectors allow specific blockade of miRNA silencing activity in mammalian developmental systems. *Front Cell Neurosci* 7: 163

Lehmann BD, Bauer JA, Chen X, Sanders ME, Chakravarthy AB, Shyr Y, Pietenpol JA (2011) Identification of human triple-negative breast cancer subtypes and preclinical models for selection of targeted therapies. *J Clin Invest* 121: 2750 – 2767

Lehmann BD, Jovanovic B, Chen X, Estrada MV, Johnson KN, Shyr Y, Moses HL, Sanders ME, Pietenpol JA (2016) Refinement of triple-negative breast cancer molecular subtypes: implications for neoadjuvant chemotherapy selection. *PLoS One* 11: e0157368

Li Y, Welm B, Podsypanina K, Huang S, Chamorro M, Zhang X, Rowlands T, Egeblad M, Cowin P, Werb Z *et al* (2003) Evidence that transgenes encoding components of the Wnt signaling pathway preferentially induce mammary cancers from progenitor cells. *Proc Natl Acad Sci USA* 100: 15853 – 15858

Liu BY, McDermott SP, Khwaja SS, Alexander CM (2004) The transforming activity of Wnt effectors correlates with their ability to induce the accumulation of mammary progenitor cells. *Proc Natl Acad Sci USA* 101: 4158 – 4163

Llobet-Navas D, Rodriguez-Barrueco R, Castro V, Ugalde AP, Sumazin P, Jacob-Sendler D, Demircan B, Castillo-Martin M, Putcha P, Marshall N *et al* (2014a) The miR-424(322)/503 cluster orchestrates remodeling of the epithelium in the involuting mammary gland. *Genes Dev* 28: 765 – 782

Llobet-Navas D, Rodriguez-Barrueco R, de la Iglesia-Vicente J, Olivan M, Castro V, Saucedo-Cuevas L, Marshall N, Putcha P, Castillo-Martin M, Bardot E *et al* (2014b) The microRNA 424/503 cluster reduces CDC25A expression during cell cycle arrest imposed by transforming growth factor beta in mammary epithelial cells. *Mol Cell Biol* 34: 4216 – 4231

Macias H, Hinck L (2012) Mammary gland development. *Wiley Interdiscip Rev Dev Biol* 1: 533 – 557

Mertelmeyer S, Weider M, Baroti T, Reiprich S, Frob F, Stolt CC, Wagner KU, Wegner M (2020) The transcription factor Sox10 is an essential determinant of branching morphogenesis and involution in the mouse mammary gland. *Sci Rep* 10: 17807

Pfefferle AD, Herschkowitz JI, Usary J, Harrell J, Spike BT, Adams JR, Torres-Arzayus MI, Brown M, Egan SE, Wahl GM *et al* (2013) Transcriptomic classification of genetically engineered mouse models of breast cancer identifies human subtype counterparts. *Genome Biol* 14: R125

Pohl SG, Brook N, Agostino M, Arfuso F, Kumar AP, Dharmarajan A (2017) Wnt signaling in triple-negative breast cancer. *Oncogenesis* 6: e310

Rajaram RD, Buric D, Caikovski M, Ayyanan A, Rougemont J, Shan J, Vainio SJ, Yalcin-Ozuysal O, Brisken C (2015) Progesterone and Wnt4 control mammary stem cells via myoepithelial crosstalk. *EMBO J* 34: 641 – 652

Rissland OS, Hong SJ, Bartel DP (2011) MicroRNA destabilization enables dynamic regulation of the miR-16 family in response to cell-cycle changes. *Mol Cell* 43: 993 – 1004

Rodriguez-Barrueco R, Nekritz EA, Bertucci F, Yu J, Sanchez-Garcia F, Zeleke TZ, Gorbatenko A, Birnbaum D, Ezhkova E, Cordon-Cardo C *et al* (2017) miR-424(322)/503 is a breast cancer tumor suppressor whose loss promotes resistance to chemotherapy. *Genes Dev* 31: 553 – 566

Sanchez-Vega F, Mina M, Armenia J, Chatila WK, Luna A, La KC, Dimitriadoy S, Liu DL, Kantheti HS, Saghafinia S *et al* (2018) Oncogenic signaling pathways in the cancer genome atlas. *Cell* 173: 321 – 337

Shirdel EA, Xie W, Mak TW, Jurisica I (2011) NAViGaTing the micronome– using multiple microRNA prediction databases to identify signalling pathway-associated microRNAs. *PLoS One* 6: e17429

Smalley MJ, Kendrick H, Sheridan JM, Regan JL, Prater MD, Lindeman GJ, Watson CJ, Visvader JE, Stingl J (2012) Isolation of mouse mammary epithelial subpopulations: a comparison of leading methods. *J Mammary Gland Biol Neoplasia* 17: 91 – 97

Wang D, Cai C, Dong X, Yu QC, Zhang XO, Yang L, Zeng YA (2015) Identification of multipotent mammary stem cells by protein C receptor expression. *Nature* 517: 81 – 84

Watson CJ (2006) Post-lactational mammary gland regression: molecular basis and implications for breast cancer. *Expert Rev Mol Med* 8: 1 – 15

Xu X, Zhang M, Xu F, Jiang S (2020) Wnt signaling in breast cancer: biological mechanisms, challenges and opportunities. *Mol Cancer* 19: 165

Yongblah K, Alford SC, Ryan BC, Chow RL, Howard PL (2018) Protecting Pax6 3' UTR from microRNA-7 partially restores PAX6 in islets from an Aniridia mouse model. *Mol Ther Nucleic Acids* 13: 144 – 153

Zhang Z, Christin JR, Wang C, Ge K, Oktay MH, Guo W (2016) Mammary-stem-cell-based somatic mouse models reveal breast cancer drivers causing cell fate dysregulation. *Cell Rep* 16: 3146 – 3156